Kawase *et al.*
Progress in Earth and Planetary Science (2023) 10:7
https://doi.org/10.1186/s40645-023-00536-4

Progress in Earth and Planetary Science

RESEARCH ARTICLE

Open Access

Historical regional climate changes in Japan in winter as assessed by a 5-km regional climate model with a land surface process

Hiroaki Kawase[1*], Shin Fukui[1], Masaya Nosaka[1], Shun-ichi I. Watanabe[1], Keishi Otomo[2], Akihiko Murata[1], Kazuyo Murazaki[1] and Tosiyuki Nakaegawa[1]

Abstract

We investigate historical regional climate changes in Japan from 1959 to 2020, analyzing a high-resolution dynamical downscaling forced by the Japanese 55-year Reanalysis (JRA-55). One-year continuous simulations are conducted by the non-hydrostatic regional climate model with a land surface model that includes the snow accumulation process, which enables us to evaluate the seasonal variation of snow cover in all of Japan. Our simulation reproduces interannual variations of the annual mean surface air temperature and annual total precipitation, and it shows rapid warming since around 1980. The annual maximum snow depth and annual maximum daily snowfall show significant decreasing trends at lower elevations on the Japan Sea sides of eastern and western Japan. Areas at higher elevations in eastern Japan show no trend in the maximum snow depth and a significant increasing trend in the maximum daily snowfall. In northern Japan, altitudinal dependencies in snow depth and snowfall changes are smaller on the Japan Sea side than on the Pacific Ocean side: the Japan Sea side shows insignificant changes in snow depth at all elevations, while the Pacific Ocean side shows decreasing and significant increasing trends at lower and higher elevations, respectively. The total number of snow-covered days is decreasing at most elevations in all regions, while the rate of decrease is smaller at higher elevations and latitudes. Composite analyses of annual maximum daily snowfall events at one prefectural city facing the Japan Sea in central Japan indicate that heavy daily snowfall occurs when the Japan Polar air mass Convergence Zone appears over the Japan Sea and the snowfall amounts show increasing and decreasing trends over the mountainous and coastal areas, respectively, due to historical warming and moistening. Our results are basically consistent with previous studies that have focused on future changes in snow depth and snowfall.

Keywords Dynamical downscaling, Regional climate model, JRA-55, Global warming, Extreme snowfall, Snow cover change

1 Introduction

According to the Intergovernmental Panel on Climate Change's Sixth Assessment Report (AR6) (IPCC 2021), it is unequivocal that human influence has warmed the atmosphere, ocean, and land. The 20-year-mean global surface temperature from 2001 to 2020 was 0.99 °C higher than that from 1850 to 1900 (IPCC 2021). In Japan, the temperature increased by 1.28 °C/100 years from 1898 to 2021 (JMA 2021), and the three recent years, 2019–2021, are the warmest since 1898. In urban

*Correspondence:
Hiroaki Kawase
hkawase@mri-jma.go.jp
[1] Meteorological Research Institute, Japan Meteorological Agency, 1-1 Nagamine, Tsukuba, Ibaraki 305-0052, Japan
[2] University of Tsukuba, Tenoudai 1-1-1, Tsukuba, Ibaraki 305-8573, Japan

areas, a much larger temperature rise has been observed because of the urban heat island (e.g., Fujibe et al. 1995; Fujibe 2009; Adachi et al. 2012).

Global warming can change the precipitation extremes. Fujibe et al. (2016) pointed out that hourly precipitation extreme values have increased at a rate to mean temperature that is slightly lower than the Clausius–Clapeyron (CC) relation rate of 6–7%/K. However, the increasing rate of water vapor due to atmospheric warming occurs in ideal conditions when the atmosphere is saturated and the synoptic-scale condition is fixed. When synoptic-scale and mesoscale water vapor convergences occur, the increasing rate of water vapor get more than the CC relation rate. Lenderink and Meijgaard (2008) demonstrated that hourly precipitation extremes increase at a rate of about 14% per K over Europe; this is known as a super or double CC relationship (Berg and Haerter 2013; Loriaux et al. 2013; Lenderink et al. 2017; Hatsuzuka et al. 2021).

In winter, snowfall and snow cover are strongly influenced by global warming. The IPCC (2021) reported that human-induced global warming has very likely contributed to the decrease in spring snow cover in the Northern Hemisphere since 1950. Rapid decreases in the annual maximum snow depth are observed at the meteorological stations in central and western Japan (JMA 2021). At low elevations in Japan, snow cover was strongly influenced by historical warming (e.g., Suzuki 2006; Ishii and Suzuki 2011; Kawase et al. 2012). In contrast, snow reductions were not observed at high-elevation meteorological stations (Suzuki 2013). Interannual variations of annual maximum snow depth differ between low elevations and high elevations (Yamaguchi et al. 2011). However, a lack of continuous observations makes it difficult to evaluate changes in snow cover over all of Japan, especially at high elevations.

Global warming promotes the conversion of snowfall to rainfall, resulting in a decrease in snowfall. On the other hand, the oceanic warming due to global warming increases water vapor in the atmosphere, contributing to an increase in snowfall if the temperature is still lower than 0 °C. Therefore, global warming has a paradox between the snowfall decrease due to warming and the snowfall increase due to moistening. In future climate conditions, snowfall is projected to largely decrease in the coastal areas of the Japan Sea (Inoue and Yokoyama 2003; Hara et al. 2008; Kawase et al. 2021), while snowfall is projected to increase over mountainous areas in central Japan and inland areas in northern Japan during mid-winter (Kawase et al. 2021). Changes in atmospheric circulation, e.g., East Asian winter monsoon and extratropical cyclone tracks, can also change winter precipitation in Japan (e.g., Hori and Ueda 2011, Kawase et al. 2015).

For evaluating the historical changes in precipitation and snow cover in Japan, a historical climate simulation with a high-resolution regional climate model is one useful method. Kayaba et al. (2016) conducted a dynamical regional downscaling of the Japanese 55-year Reanalysis (JRA-55) (Kobayashi et al. 2015), named DSJRA-55, which covers all of Japan for the 55 years from 1958 to 2012 with a 5-km grid spacing. However, it lacks continuity over time because its initial and boundary conditions are renewed every 6 h. The land surface model for DSJRA-55 includes no snow accumulation process. Thus, DSJRA-55 cannot evaluate historical changes in snow cover and related variables. To evaluate the regional characteristics of extreme snowfall in Japan, Kawase et al. (2018) conducted 5-km simulations using a regional climate model including a land surface process based on JRA-55 and historical experiments of the database for Policy Decision-making for Future climate change (d4PDF) (Mizuta et al. 2017). However, their simulations were conducted from 1981 to 2010 and did not cover the northern part of Japan, Hokkaido, and the southwestern island, Okinawa.

In this study, we conducted a dynamical downscaling of JRA-55 using a 5-km regional climate model with a snow accumulation process covering all of Japan from 1958 to 2020. In the dynamical downscaling, time integrations were continuously performed without frequent reinitializations. The downscaling data enable us to evaluate long-term changes in annual maximum snow depth in the whole of Japan in addition to changes in air temperature and precipitation. The purpose of this study is to investigate historical changes in winter precipitation and snow cover using the 5-km regional climate model. Our experimental designs are shown in Sect. 2. We describe the reproducibility of historical changes in regional climate in Japan—including snowfall and snow depth—as compared with in situ observations and DSJRA-55. We also evaluate the altitudinal dependency of historical snow cover changes in each region, which has not been evaluated because of a lack of snow observations at high elevations. We show an example of the analysis of the historical trend in heavy daily snowfall and discuss the trends of background conditions on heavy snowfall days in Sect. 4. Section 5 summarizes our results.

2 Methods/experimental design

A dynamical downscaling of the JRA-55 was conducted to produce a regional climate dataset over Japan with a grid spacing of 5 km from September 1958 to August 2021. We use the non-hydrostatic regional climate model (NHRCM, Sasaki et al. 2008) developed by the Meteorological Research Institute (MRI) of the Japan Meteorological Agency (JMA). The double nesting was applied here

by downscaling from JRA-55 to a horizontal grid spacing of 20 km covering the Far East and further by downscaling from the result to a horizontal grid spacing of 5 km covering Japan (hereafter, referred to as DS20km and DS5km, respectively) (Fig. 1). The model tops are set to 22 km with 50 terrain-following layers in NHRCMs with both horizontal grid spacings.

For representing physical processes, the NHRCM includes the Kain–Fritsch cumulus parameterization (Kain and Fritsch 1990; Kain 2004; Nakano et al. 2012), the bulk cloud microphysics scheme predicting the mixing ratios of five hydrometeor species and the number concentrations of three ice-phase hydrometeor species (Ikawa and Saito 1991); the Mellor–Yamada–Nakanishi–Niino level-2.5 turbulence closure model (Nakanishi and Niino 2004), the radiation schemes for clear skies (Yabu et al. 2005) and clouds (Kitagawa 2000); and the improved MJ-SiB (Hirai et al. 2007) (iSiB), which is a land surface model with a snow accumulation sub-model based on the simple biosphere model (Sellers et al. 1986) with surface bulk coefficients provided by Beljaars and Holtslag (1991).

Spectral nudging (von Storch et al. 2000; Nakano et al. 2012) is applied, in addition to forcing from lateral boundaries. The components for spectral nudging are longer than 800 km in wavelengths with heights above 2 km in the DS20km, while they are longer than 500 km in wavelength with heights above 7 km in the DS5km. The land use is derived from the global land cover characterization (GLCC), which is fixed throughout the period. Grids where the sea surface temperature is less than 271 K are assumed to be covered with sea ice. The concentrations of greenhouse gases (GHGs)—specifically CO_2, CH_4, and N_2O—are updated every year. Note that GHG concentrations are based on representative concentration pathway 8.5 (RCP8.5) from 2005. The CO_2 concentrations in RCP8.5 agree most closely with historical ones—within 1% from 2005 to 2020 (Schwalm et al. 2020). The specifications of the numerical settings are summarized in Table 1.

To cover the long term, the dynamical downscaling is split into streams. Each stream is set to cover 1 year—from September to the following August—with a continuous time integration. Each year, the DS20km and DS5km are initialized at 12 UTC on July 20 and 21, respectively. Our experiments have spin-up durations of approximately 40 days. To distinguish it from DSJRA-55 (Kayaba et al. 2016), our simulation was called regional climate downscaling using JRA-55 (RCDSJRA-55), which includes DS20km and DS5km.

DS5km is compared with in situ long-term observations operated by the JMA from 1959 to 2020. We used 15, 51, and 30 stations for air temperature, precipitation, and snow depth, respectively. The locations of the stations are shown in Fig. 1b. We also used AMeDAS information after 1976 to evaluating the climatological temperature and precipitation biases. The AMeDAS network has approximately 1300 points that observe precipitation in Japan (figure not shown). Approximately two-thirds of AMeDAS stations observe surface air temperature and wind. For comparing with the observations, the grid points near the observational stations are extracted from DS5km. DS5km is also compared with DSJRA-55. Climatology is defined as the 30-year averages from 1991 to 2020 or from 1981 to 2010 because of the limitation of DSJRA-55. In the analysis of snowfall and snow cover, annual values are calculated from September to December of the preceding year and from January to August of the target year, i.e., the annual maximum snow depth in 1962 means the maximum snow depth from September 1961 to August 1962, which is the same as the JMA's definition.

3 Results

3.1 Climatological biases and historical variations of air temperature and precipitation

Figure 2 shows biases of surface air temperature and precipitation in DS5km to the AMeDAS observation. Note that the air temperature biases derived from the difference of surface heights between AMeDAS and the nearest model grid point were modified using the dry adiabatic lapse rate. Annual surface air temperatures show small biases in most parts of Japan, while DJF surface air temperatures have cold biases, especially in eastern and northern Japan (Fig. 2a, b). The cold and warm biases in cold and warm seasons, respectively, are almost canceled out (Fig. 3a, b). Kayaba et al. (2016) showed that DSJRA-55 had similar temperature biases in eastern and northern Japan, i.e., cold temperature biases in January and warm temperature biases in August.

The annual total precipitation shows small biases at most stations, with the exception of inland stations in central Japan (Fig. 2d). The positive biases at the inland stations in the central parts of Japan are derived from the overestimation of summer precipitation (figure not shown). The total DJF precipitation, on the other hand, shows large positive biases over the inland areas along the Pacific Ocean and negative biases over the coastal areas along the Japan Sea (Fig. 2e). Note that the amount of winter precipitation along the Pacific Ocean is much smaller than that along the Japan Sea (figure not shown).

Figure 3 shows the climatology and biases of the monthly mean surface air temperature and precipitation. DS5km shows cold and warm biases in cold and warm seasons, respectively, while DSJRA-55 shows relatively small warm biases in all seasons (Fig. 3a, b). Different

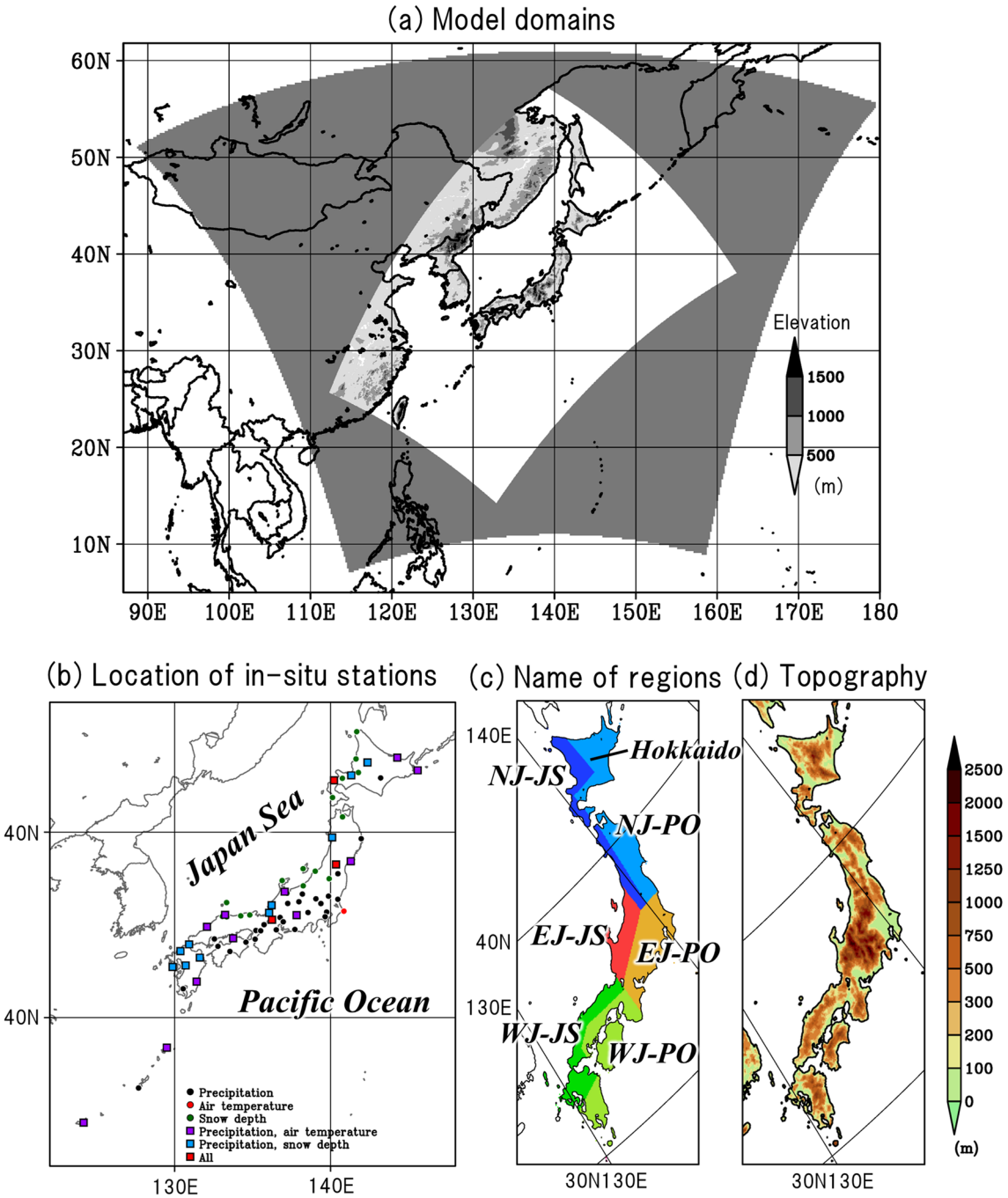

Fig. 1 Model domains, locations of observational stations, Japanese regions, and topography. **a** The gray-shaded region is the first domain of the NHRCM with 20-km grid spacing. The inner region shows the second domain of the NHRCM with 5-km grid spacing. The gray and black gradation in the second domain shows the topography. **b** Locations of in situ stations. Black, red, and green circles represent stations measuring precipitation, air temperature, and snow depth, respectively. Purple, light blue, and red squares represent stations measuring both precipitation and air temperature, both precipitation and snow depth, and all three variables, respectively. **c** Japanese regions with their naming of a combination of NJ/EJ/WJ and JS/PO: The former denotes northern, eastern, and western Japan, and the latter denotes the Japan Sea and Pacific Ocean sides. These regions are based on those delineated by Murata et al. (2015). **d** Topography in Japan except for southwestern islands

Table 1 Specifications of the numerical model

	20 km NHRCM	**5 km NHRCM**
Grid number	281 × 281 × 50	527 × 804 × 50
Time interval	60 s	20 s
Initial and lateral boundary condition	JRA-55 (Kobayashi et al. 2015)	20 km NHRCM
Initial date	July 20	July 21
Target years	From September 1958 to August 2020 First 40 days (July 21–August 31) are spin-up durations for NHRCM with 5 km grid spacing	
Topography	GTOPO30 (grid mean)	
Microphysics	Prognostic variables: mixing ratio (water vapor, cloud water, cloud ice, snow, and graupel) and number concentration (cloud ice, snow, graupel) (Ikawa and Saito 1991)	
Boundary layer	MYNN level 2.5 (Nakanishi and Niino 2004)	
Cumulus convection	KF scheme (Kain and Fritsch 1990; Kain 2004; Nakano et al. 2012)	
Radiation	Clear sky (Yabu et al. 2005) and cloud (Kitagawa 2000)	
Land surface	Improved MJ-SiB (Hirai et al. 2007)	
Wave number boundary of spectral nudging	Wave length: longer than 800 km Height: over 2 km above sea level (von Storch et al. 2000; Nakano et al. 2021)	Wave length: longer than 500 km Height: over 7 km above sea level

surface models between DS5km and DSJRA-55 can produce the difference in surface air temperature biases. On the other hand, both DS5km and DSJRA-55 show similar seasonal variation in precipitation biases (Fig. 3c, d) and DS5km shows smaller and larger precipitation biases in warm and cold seasons, respectively, than those in DSJRA-55. DS5km can reproduce large amounts of precipitation from June to September better than those of DSJRA-55. A short spin-up duration in DSJRA-55 may result in the underestimation of precipitation in warm seasons.

The grid-mean topography is smoother than the realistic topography. The mountain heights in the model are lower than the actual mountain heights, resulting in the underestimation of topographical precipitation on the windward side of the mountains. Variables in the regional climate model, such as precipitation, air temperature, and wind, are the averaged values in each grid point, which is different from the variables observed just at the observation site; this also causes the model biases. Moreover, in winter, convective precipitation develops over the Japan Sea, which is developed by the warm Japan Sea and the cold air mass from the continent. In this situation, the planetary boundary layer (PBL), cumulus convection, and microphysics scheme are important for reproducing the winter precipitation over the Japan Sea side. The overestimation of winter precipitation can be derived from these parameterization schemes in the NHRCM. Moreover, the horizontal grid spacing of 5 km is too coarse to resolve the cumulus convections over the Japan Sea, which results in less precipitation over coastal and more precipitation over mountainous areas along the Japan Sea (Kawase et al. 2019). The fact that the mountain ranges in the model are lower than the actual ones also causes negative and positive biases of winter precipitation over mountainous areas of the Japan Sea and the Pacific Ocean sides, respectively (Ishizaki et al. 2012; Kawase et al. 2015).

DS5km well reproduces the interannual variations of surface air temperature from 1959 to 2020 observed by the 15 in situ stations as with DSJRA-55 (Fig. 4a). Correlation coefficients between DS5km (DSJRA-55) and observations are 0.981 (0.965) and 0.992 (0.970) in annual and 5-year running mean temperatures, respectively. The recent rapid warming since about 1980 is well reproduced by DS5km and DSJRA-55. Linear trends of the annual mean temperature are 1.25 °C and 0.92 °C per 60 years for the observations and the DS5km, respectively, with a 99% confidence level. As with the annual mean temperature, the annual and 5-year running mean total precipitation shows high correlations with DS5km (0.877 and 0.822) and with DSJRA-55 (0.936 and 0.919), respectively. Since the DS5km underestimates the annual total precipitation in the 1970s, the correlation is lower than that of DSJRA-55 (Fig. 4b). Annual total precipitation shows increasing trends in DS5km and the observation, although both are statistically insignificant.

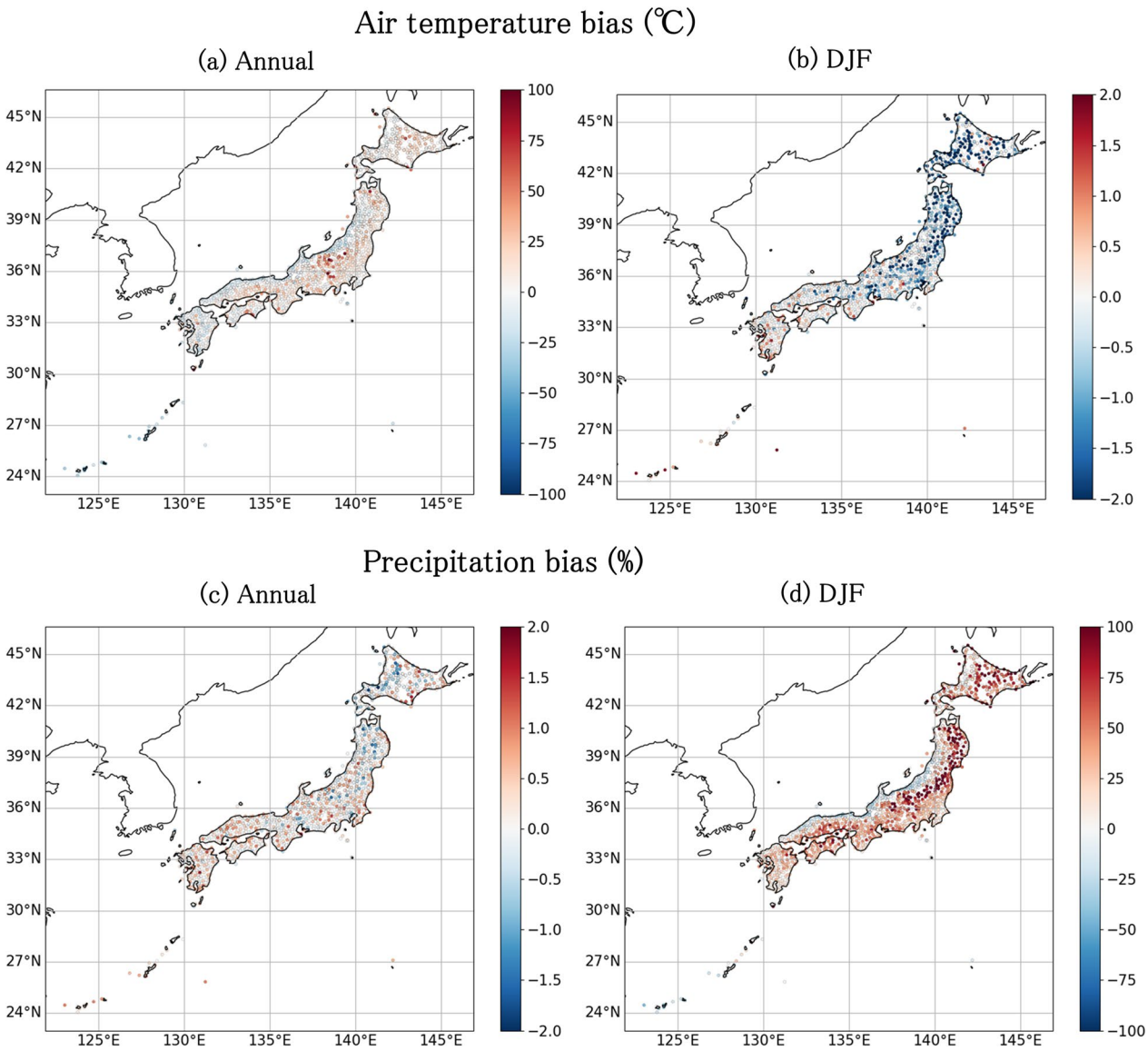

Fig. 2 **a**, **b** Surface air temperature and **c**, **d** precipitation biases based on AMeDAS observations averaged between 1991 and 2020; **a** annual and **b** DJF mean air temperature biases; **c** annual and **d** DJF total precipitation biases shown as percentages

DS5km is also highly capable of simulating interannual variations of precipitation extremes, such as daily precipitation exceeding 100 mm/day (hereafter, referred to as nPR100) and annual maximum daily precipitation (hereafter, referred to as Rx1d) (Fig. 4c–d). The correlation coefficient of nPR100 between DS5km (DSJRA-55) and the observation is 0.638 (0.758) for annual values and 0.649 (0.695) for 5-year running mean values. Both the observation and DS5km show increasing trends (0.34 and 0.23 days/60 years) with 95% and 90% confidence levels, respectively (Fig. 4c). Rx1d also shows a similar interannual variation between the observation and DS5km and DSJRA-55. The observed Rx1d shows an increasing trend (10.57 mm/60 year) with a 90% confidence level, while the trends simulated by DS5km and DSJRA-55 are not statistically significant (Fig. 4d). The extreme daily precipitation in Japan mainly occurs in summer. Since this study focuses on the historical chances in winter precipitation and snow cover in Japan, the detailed analyses of historical changes in extreme precipitation in summer would be the future studies.

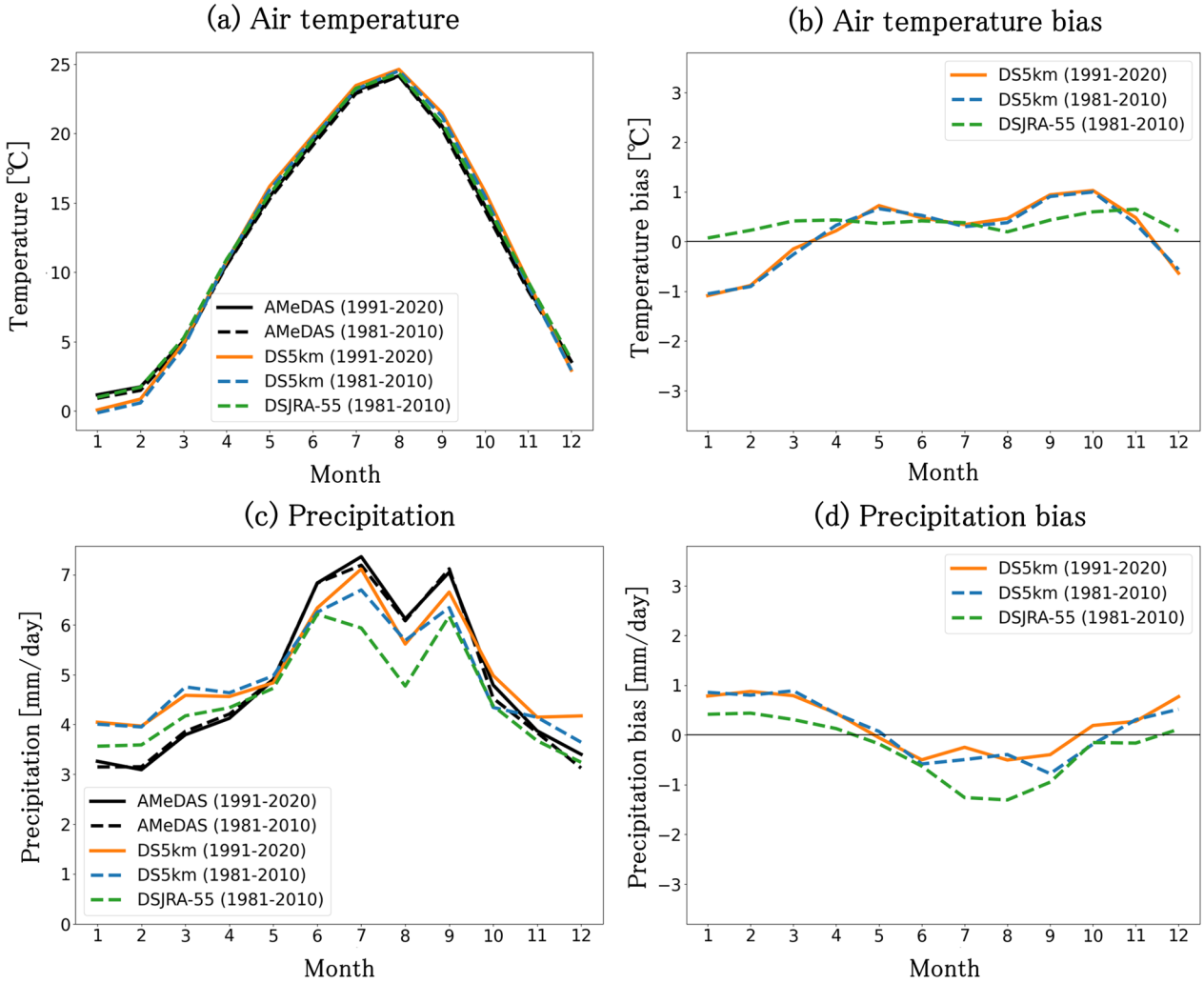

Fig. 3 Monthly mean surface air temperature and monthly precipitation; **a** mean surface air temperature and their biases; **c**, **d** total precipitation and their biases; **a**, **c** black and orange lines represent the averages of AMeDAS and DS5km, respectively, between 1991 and 2020. Blue and green lines represent the averages of DS5km and DSJRA-55, respectively, between 1981 and 2010. **b**, **d** Orange, blue, and green lines represent the biases in DS5km (1991–2020), DS5km (1981–2010), and DSJRA-55 (1981–2010), respectively

(See figure on next page.)

Fig. 4 Interannual variations of air temperature and precipitation in all of Japan from 1959 to 2020. **a** Surface air temperature, **b** annual total precipitation, **c** annual frequency of daily precipitation exceeding 100 mm/day (nPR100), and **d** annual maximum daily precipitation (Rx1d). Thick and thin lines represent annual and 5-year means, respectively. Black and gray, red and light red, and blue and light blue lines represent observations, DS5km, and DSJRA-55, respectively. The temperature and precipitation are averaged from 15 and 51 stations shown in Fig. 1b or grid points near the stations, respectively

3.2 Historical changes in annual maximum snow depth and daily snowfall

As compared to the DSJRA-55, the biggest advantage of the DS5km is in evaluating historical snow cover with a 5-km grid spacing for all of Japan. First, we compare the reproducibility in annual maximum snow depth (hereafter, referred to as SDmax) in DS5km with in situ observations by the JMA. Figure 5 shows the time series of SDmax anomalies relative to 1991–2020 on the Japan Sea side, which has large amounts of snowfall. Note that most stations observing snow depth over the long term are located at low elevations (Fig. 1b). As with the previous figures, the grid points in DS5km

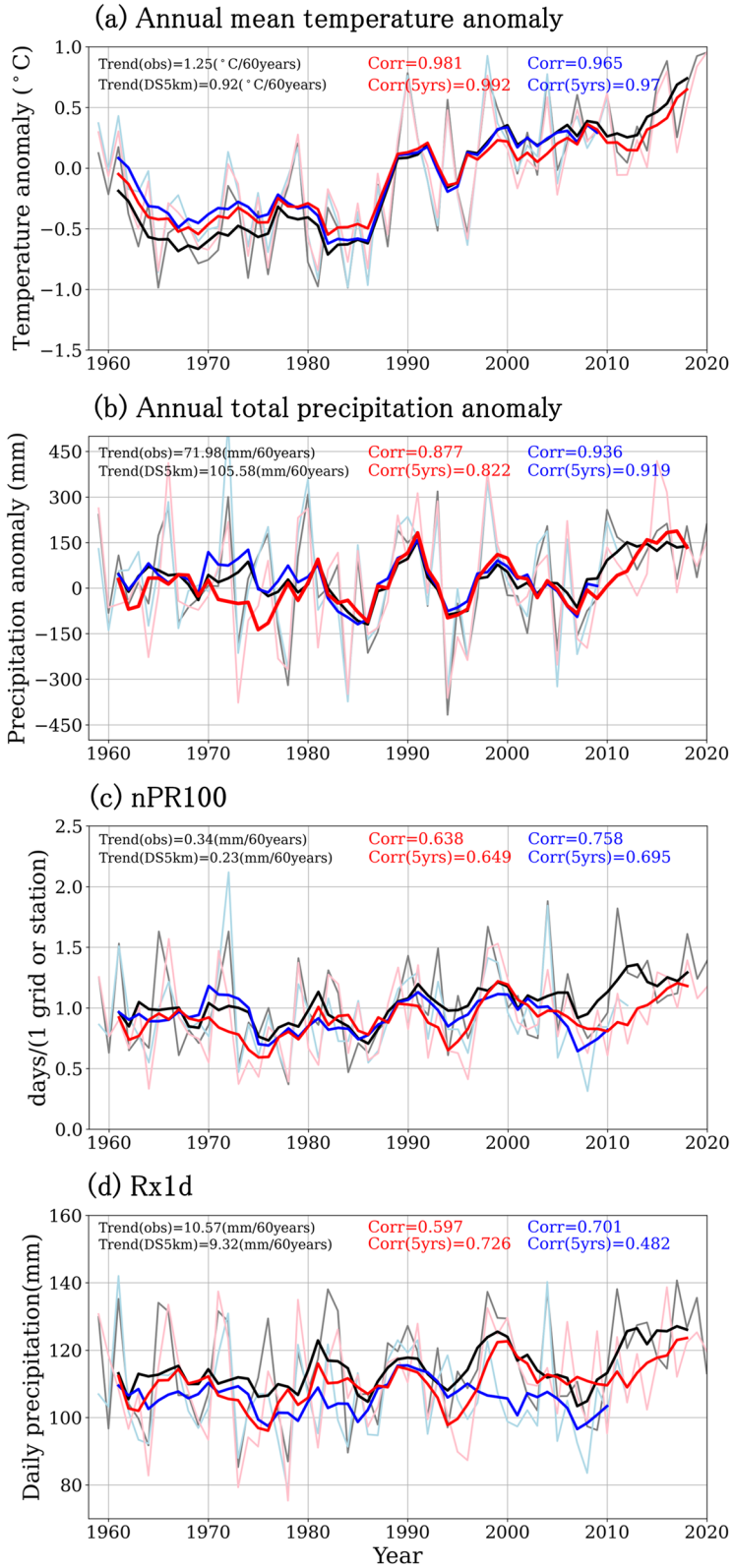

Fig. 4 (See legend on previous page.)

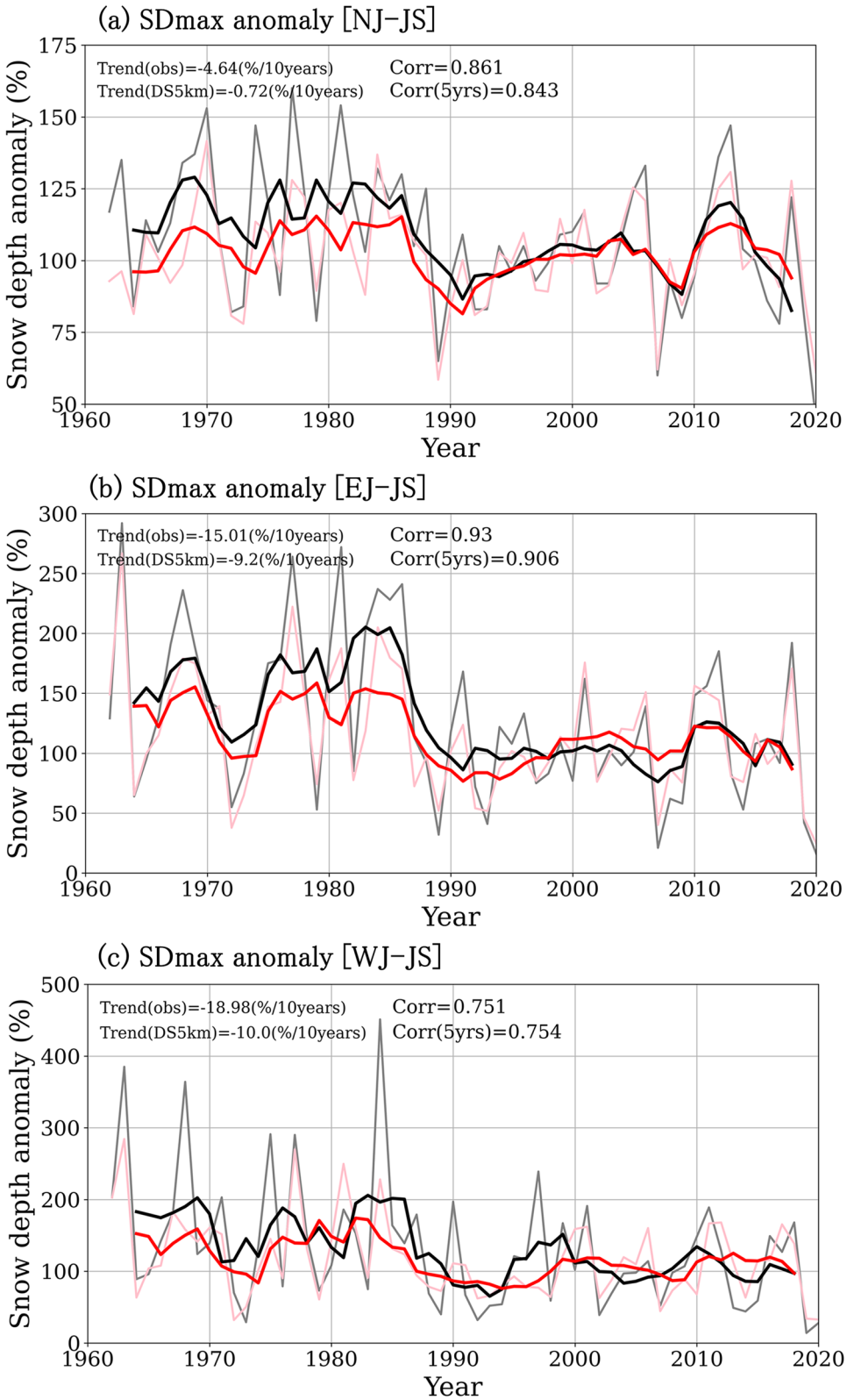

Fig. 5 Time series of SDmax anomalies over the Japan Sea coast from 1962 to 2020. **a** Northern Japan, **b** eastern Japan, and **c** western Japan. The reference climate is 1991–2020. Thick and thin lines represent the annual and 5-year means, respectively. Black and red lines represent the observation and DS5km, respectively

near the snow observational stations are extracted and averaged in each region.

The observed SDmax shows decreasing trends in all regions. Eastern and western Japan shows large decreasing trends (−15.0% and −19.0%/10 years, respectively). The decreasing trend in northern Japan (−4.6%/10 years) is smaller than those in other regions. All decreasing trends are statistically significant with a 95% or 99% confidence level. DS5km also shows decreasing trends in eastern and western Japan (−10.0% and −9.2%/10 years, respectively) with a 95% confidence level, although the decreasing trends are smaller than the observed ones. On the other hand, the decreasing trend is quite small and statistically insignificant in northern Japan. The difference between the SDmax before 1990 and after 1991 is relatively smaller in DS5km than that in the observation, resulting in the smaller decreasing trends in DS5km.

Figure 6a shows the interannual variation of the annual maximum daily snowfall (hereafter, referred to as Sx1d) at 30 stations shown in Fig. 1. Here, daily snowfall is calculated by hourly increments of snow depth, which is the same definition used by the JMA. The Sx1d simulated by DS5km is smaller than the observation. On the other hand, the annual variation has a high correlation coefficient (0.768) between the observation and DS5km. DS5km shows decreasing trends, which are opposite to the trends of the Rx1d (Fig. 4d), while they are statistically insignificant. Note that the JMA measured daily snowfall using a snow board before around 1997–2004, which was different from the current method. Since the change in measurement influences a long-term trend of daily snowfall, we did not discuss the long-term trends of observed daily snowfall. Figure 6b–d shows the annual variations of the Sx1d anomaly in each region as with SDmax in Fig. 5. The correlation of annual variations in the Sx1d anomaly is higher in western Japan and lower in northern Japan between the observation and DS5km, which could be derived from the lower and higher frequencies of snowfall in northern Japan and western Japan, respectively. Generally, the heavy snowfall on Japan Sea coast in western Japan is brought by the Japan Polar air mass Convergence Zone (JPCZ), which is generated by a convergence of northwesterly winds circumventing the Changbai Mountains on Korean Peninsula. Our results show that the reproducibility of heavy snowfall events derived from the JPCZ would be better.

3.3 Altitudinal dependency of historical snow cover changes

Snowfall and snow depth are strongly influenced by air temperature, especially at approximately 0 °C, meaning that elevation is an important factor when considering historical changes in snowfall and snow depth. Climatology of SDmax exceeds 150 cm over the mountainous areas in eastern and northern Japan (Fig. 7a). Table 2 summarizes climatology of SDmax at each elevation range in each region. Above 1000 m, SDmax exceeds 300 cm in northern Japan and exceeds 250 cm in eastern Japan. Both decreasing and increasing trends are simulated by DS5km (Fig. 7b), while most trends are statistically insignificant in each grid except for western Japan. We evaluated the annual variations of regional mean SDmax from low elevations (0–250 m) to high elevations (1000–1500 m or over 1500 m). SDmax shows similar variations at all elevations on the Japan Sea side of northern Japan, and no significant trends were detected (Fig. 8a). On the other hand, on the Japan Sea side of eastern Japan, SDmax shows a decreasing trend more clearly at lower elevations, as with observations (Fig. 5), and no trend or increasing trends at higher elevations (Fig. 8c). In western Japan, all elevations show decreasing trends in SDmax, with a 95% confidence level. As stated in previous studies (Suzuki 2006; Ishii and Suzuki 2011; Kawase et al. 2012), SDmax can be largely decreased by historical warming at the lower elevations in eastern and western Japan where the surface air temperature is around 0 °C even in winter.

Short-term heavy snowfalls bring risks of traffic hindrances, the isolation of villages through road closures, collapse of houses, and surface avalanches in mountainous areas. Compared with SDmax, the altitudinal dependency of Sx1d is smaller (Fig. 7c). Sx1d widely exceeds 20 cm in most areas of northern Japan and in some parts of eastern and western Japan, especially the areas facing the Japan Sea. Note that Sx1d over 20 cm is also found in the mountainous areas of western Japan facing Pacific Ocean. Heavy daily snowfall occurs over the mountainous areas in eastern Japan and the northern part of Japan (Hokkaido). Long-term trends of Sx1d are similar to those of SDmax (Fig. 7d). Increasing trends are found more widely in eastern and western Japan. As with SDmax, most trends are statistically insignificant in each grid, except for the coastal areas along the Japan Sea in western Japan. Figure 9 shows the interannual variations and trends in Sx1d. In the Japan Sea side of northern Japan, all elevations show increasing trends, especially at higher elevations above 1000 m (1.40%/10 years), although they are not statistically significant (Table 2). The Pacific Ocean side of northern Japan has large interannual variations of Sx1d, and the variations differ among the elevations (Fig. 9b). As with the Japan Sea side, all elevations except for 0–250 m show increasing trends of Sx1d, and elevations higher than 1500 m show a significant increasing trend with a 90% confidence level (Table 2).

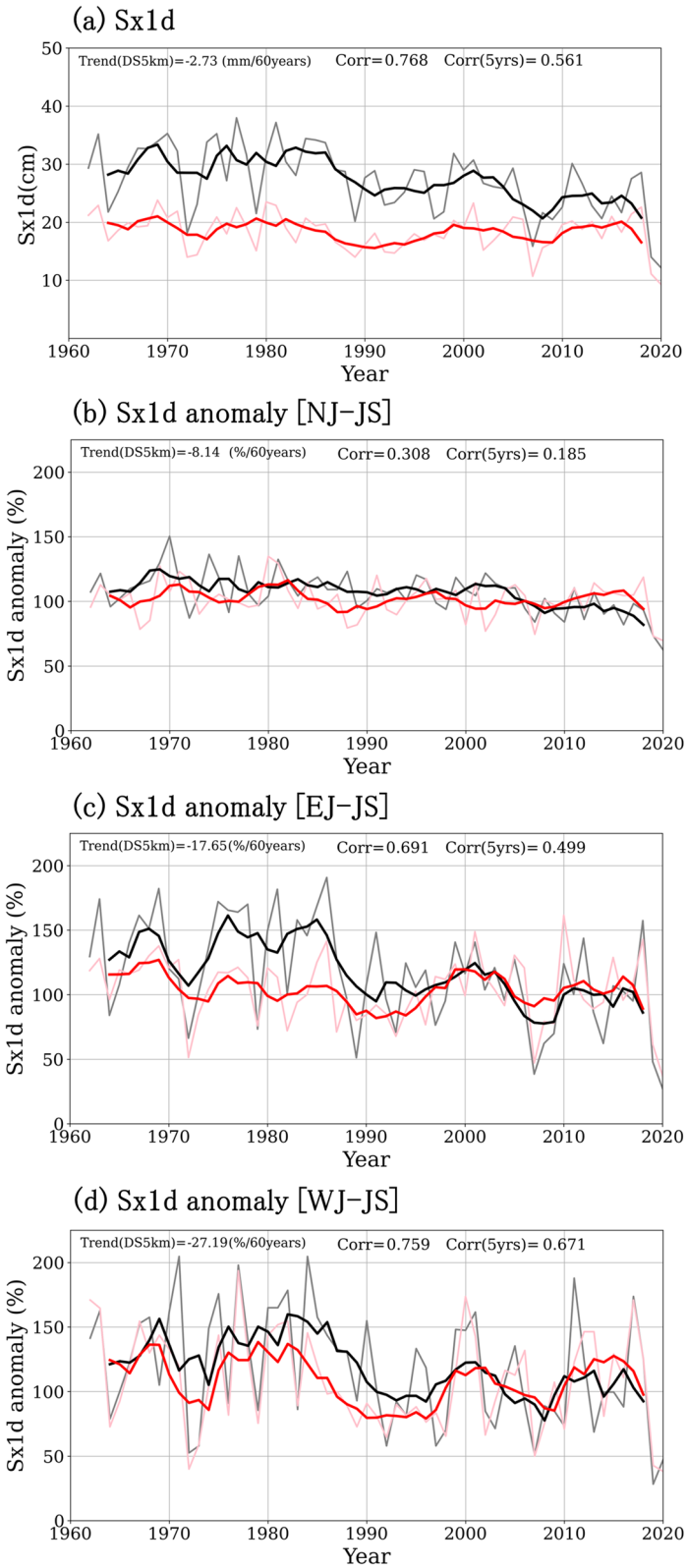

Fig. 6 **a** Same as Fig. 4, but Sx1d without an observed trend; **b**–**d** same as Fig. 5, but Sx1d without observed trends

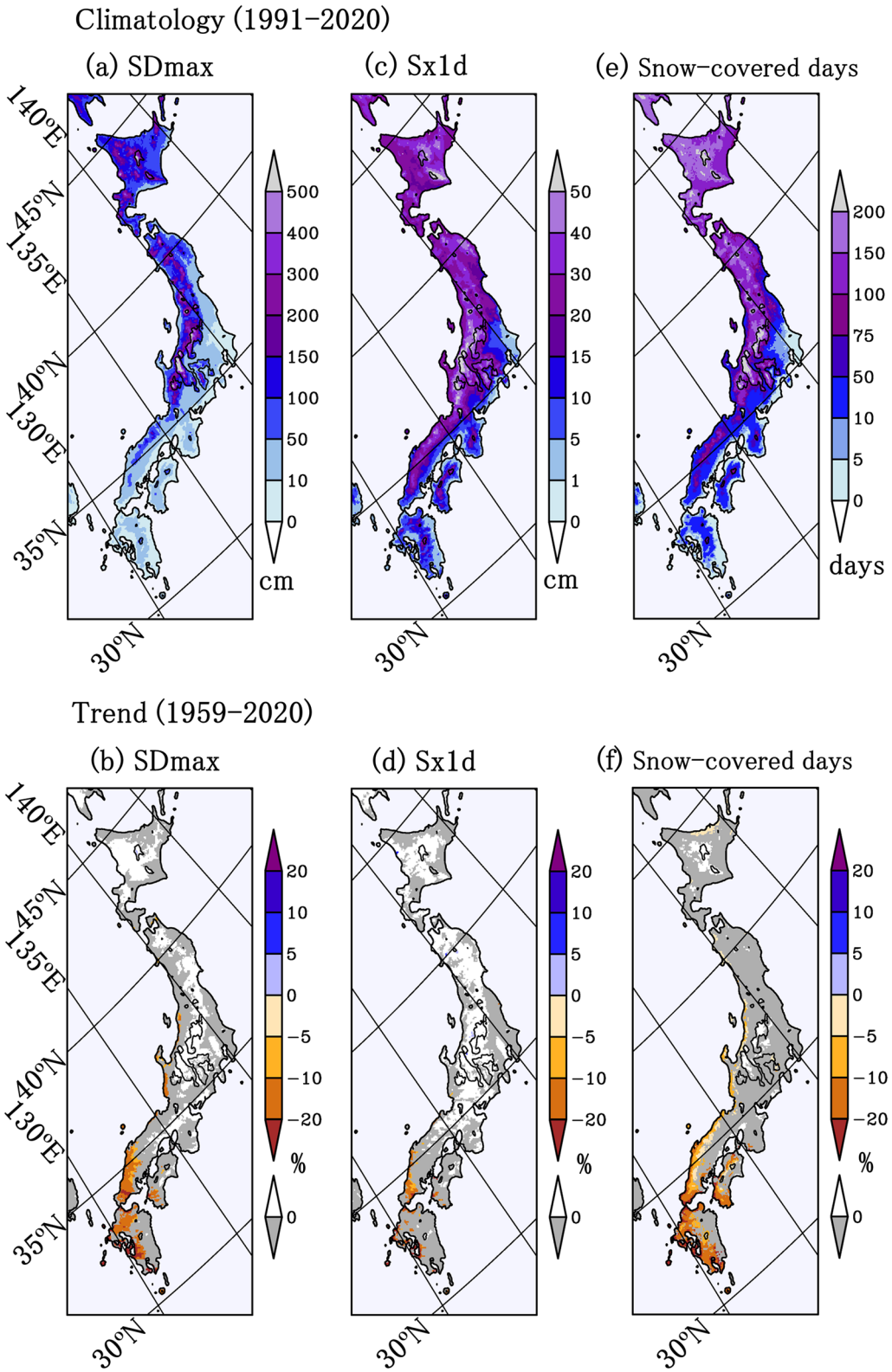

Fig. 7 Climatology in 1991–2020 and linear trends from 1959 to 2020. **a**, **c**, **d** Climatology of SDmax, Sx1d, and snow-covered days, respectively; **b**, **d**, **f** linear trends of SDmax, Sx1d, and snow-covered days, respectively. Gray and white shadings represent decreasing and increasing trends, respectively, which are statistically insignificant with a 95% confidence level

Table 2 SDmax and Sx1d climatology and linear trends

Elevation(m)	SDmax climatology (cm) (1991–2020)				Sx1d climatology (cm) (1991–2020)			
	NJ–JP	NJ–PO	EJ–JS	WJ–JS	NJ–JP	NJ–PO	EJ–JS	WJ–JS
0–250	89.5	59.7	49.6	13.1	22.9	25.0	26.1	9.3
250–500	142.6	93.8	103.7	31.6	28.6	31.1	36.9	19.4
500–1000	230.5	157.7	161.1	54.7	36.3	37.2	40.6	25.4
1000–1500	326.6	320.9	275.4	41.8	43.3	44.4	45.6	26.9
1500–		667.2	443.0			63.4	50.6	
	SDmax trend [%/10 years]				**Sx1d trend [%/10 years]**			
0–250	−0.92	−1.02	−8.70***	−11.25***	0.11	−0.32	−2.24	−6.97***
250–500	−0.34	−0.46	−3.77	−7.48**	0.42	0.12	−0.18	−3.43**
500–1000	−0.36	−0.20	−0.98	−5.90**	0.52	0.26	0.79	−2.42*
1000–1500	−0.37	1.00	0.04	−7.62**	1.40	0.96	1.46*	0.12
1500–		2.40**	1.10			2.23*	1.39	

One, two, and three asterisks mean a statistical significance with 90%, 95%, and 99% confidence levels, respectively

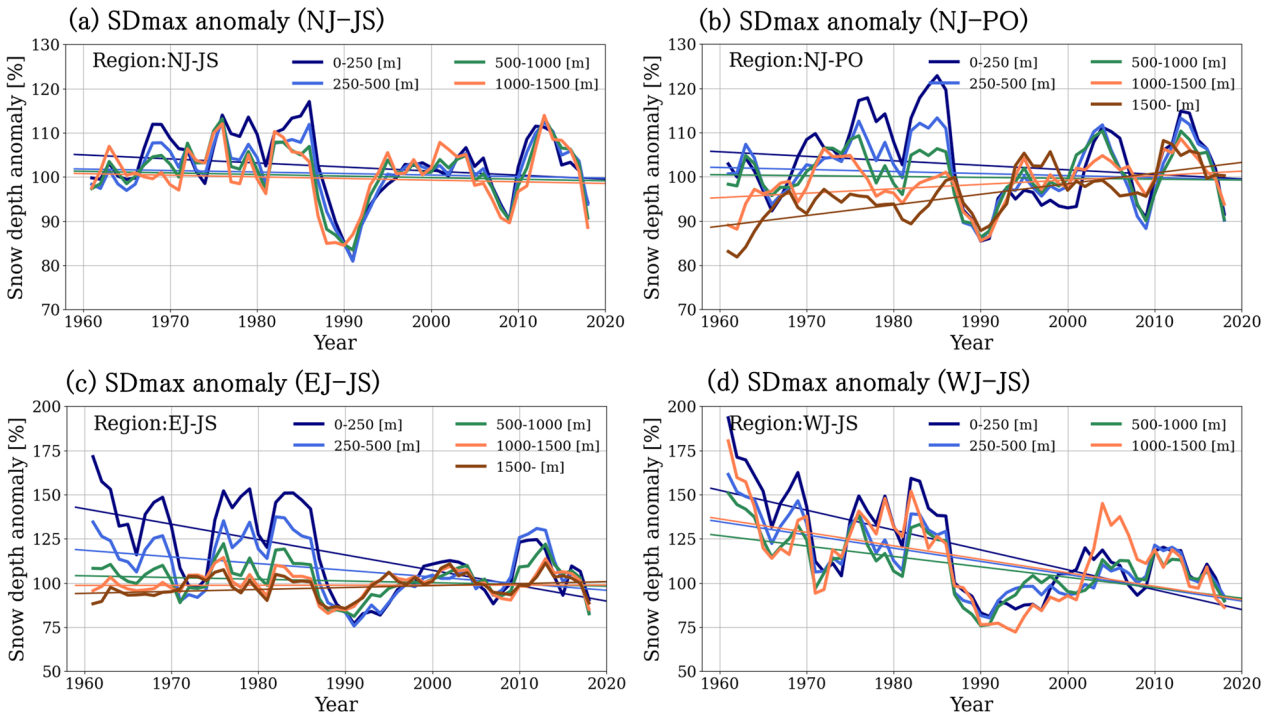

Fig. 8 Annual variations and linear trends of SDmax anomalies relative to 1991–2000 at 0–250 m (blue line), 250–500 m (light blue line), 500–1000 m (green line), 1000–1500 m (orange line), and over 1500 m (brown line). The straight lines represent linear trends

Sx1d of eastern Japan has a clear elevation dependency, which is similar to those of SDmax (Fig. 9c). In contrast to SDmax, the decreasing trend at the lowest elevations is insignificant, and higher elevations show significant increasing trends with 90% and 95% confidence levels (Table 2). These results are consistent with the enhancement of daily snowfall extremes in the mountainous areas due to global warming (Kawase et al. 2016, 2021). In western Japan, the decreasing trends of Sx1d are significant at elevations lower than 1000 m, but the decreasing trends are smaller than those of SDmax. At elevations higher than 1000 m, the Sx1d shows insignificant decreasing trends, although SDmax shows a significant decreasing trend.

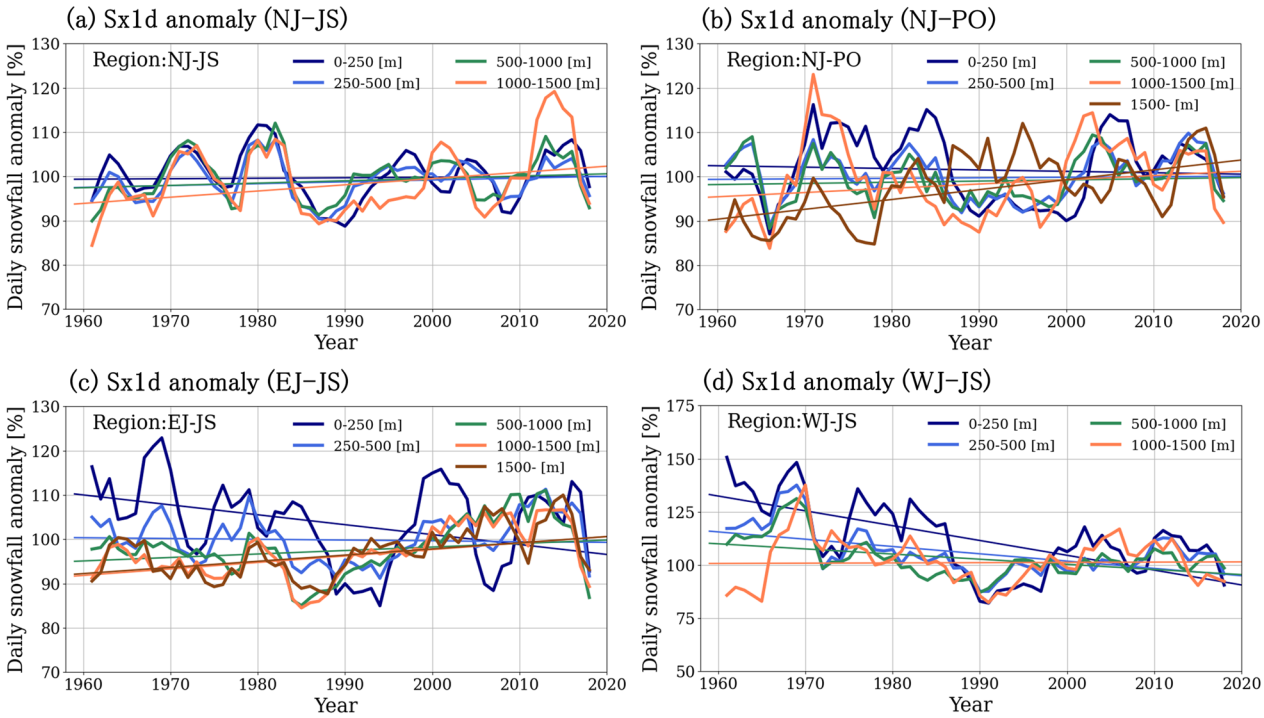

Fig. 9 Same as in Fig. 8, but Sx1d

3.4 Synoptic conditions of heavy snowfall events on the Japan Sea and Pacific Ocean sides of northern Japan, Hokkaido

Generally, the total snowfall on the Pacific Ocean side of Japan is much less than that on the Japan Sea side. The mean SDmax in EJ–PO and WJ–PO is 8.6 cm and 5.2 cm, respectively, at elevations of 0 to 250 m, which are much less than those in EJ–JP and WJ–JP (49.6 and 13.1 cm, respectively) (Table 2). On the other hand, the Pacific Ocean side of northern Japan has plenty of snow depth as compared with EJ–PO and WJ–PO at lower elevations (Table 2) and is comparable to that on the Japan Sea side at higher elevations. Sudden heavy snowfall can collapse wooden and unmanaged houses because of the snow load, which mainly occurs in regions with infrequent snowfall, such as on the Pacific Ocean side. It is noteworthy that the trends and variations in SDmax and Sx1d strongly depend on the elevation on the Pacific Ocean sides of northern Japan (Figs. 8b, 9b, respectively), in contrast to that on the Japan Sea side (Figs. 8a, 9a, respectively).

On the Pacific Ocean side of northern Japan, extratropical cyclones passing around northern Japan bring heavy snowfall (Inatsu et al. 2021). In this synoptic condition, warm and moist air masses are transported from the warm Pacific Ocean to northern Japan. On the other hand, heavy snowfall occurs on the Japan Sea side of northern Japan when cold air breaks out. Figure 10 shows the composites of precipitation, surface wind, sea-level pressure (SLP), and surface air temperature in Sx1d events at Rumoi (Fig. 10a, b) and at Obihiro (Fig. 10c, d) in Hokkaido. The composite of heavy snowfall events in Rumoi shows that the northerly wind prevails and a cold air advection occurs northeast of Rumoi. The daily mean air temperature is lower than −6 °C over most parts of Hokkaido. On the other hand, the composite of heavy snowfall events in Obihiro shows that the southeasterly prevails and warm air advection occurs southeast of Obihiro. The daily mean air temperature is higher than −6 °C with the exception of high elevations. Large amounts of precipitation are widely simulated over the eastern parts of Hokkaido. These results are consistent with those of Inatsu et al. (2021), and the air temperature on the Pacific Ocean side is relatively higher than that on the Japan Sea side when heavy snowfall occurs. Historical global warming (Fig. 4a) promotes the conversion from snowfall to rainfall if the air temperature is around 0 °C. The air temperature at lower elevations is close to 0 °C when snowfall occurs at low elevations in NJ–PO, while the air temperature is much lower than 0 °C at high elevations (Fig. 10d). Therefore, the NJ–PO shows the large

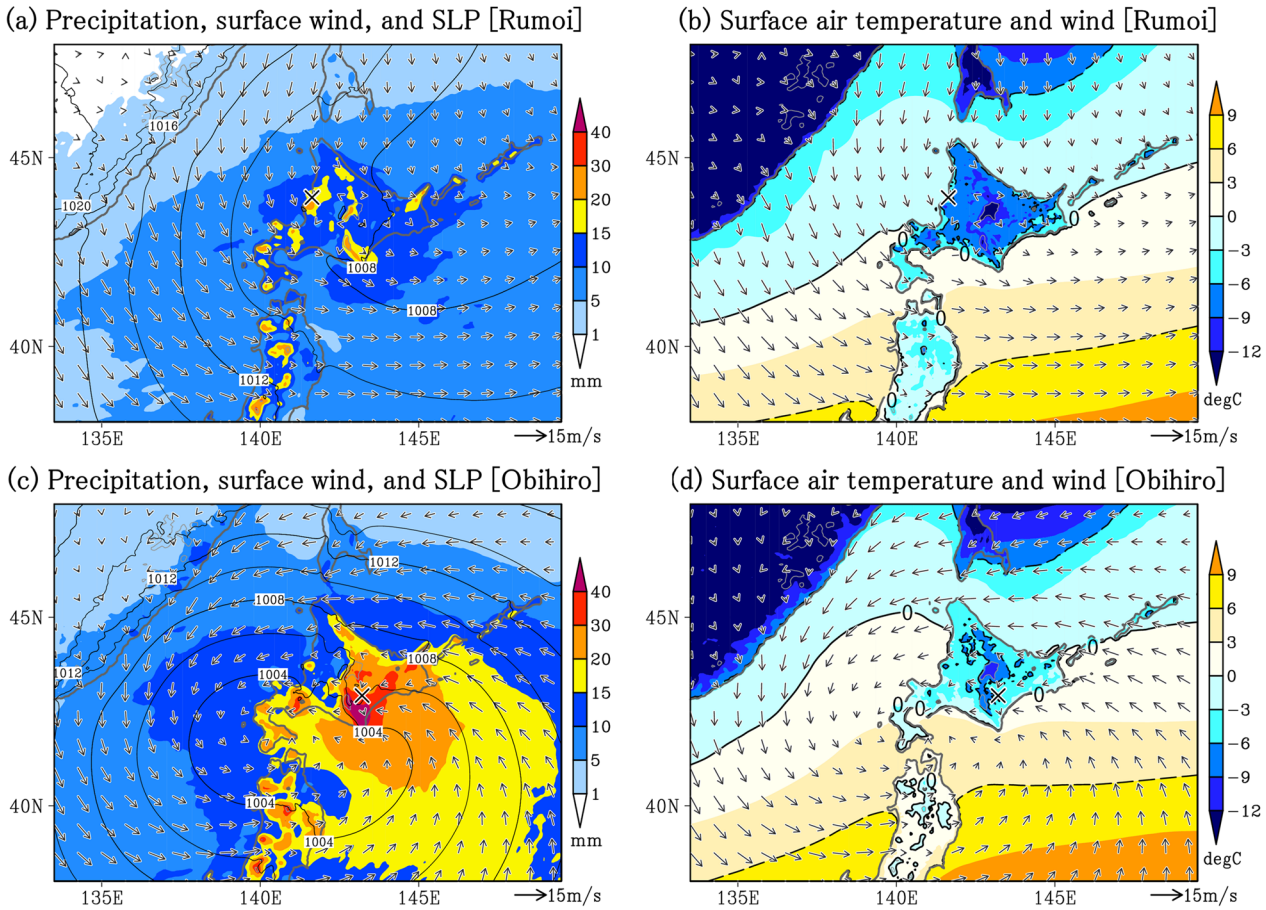

Fig. 10 Composites of precipitation, surface wind, SLP, and surface air temperature when Sx1d is calculated in DS5km at Rumoi and Obihiro. **a**, **c** Precipitation, surface wind, and SLP; **b**, **d** surface air temperature and surface wind; **a**, **b** Rumoi and **c**, **d** Obihiro. Cross marks represent the locations of Rumoi and Obihiro

elevation dependency of SDmax as compared with the NJ–JS.

3.5 Historical changes in snow-covered days

Finally, we investigate changes in the number of days with snow cover. Here, we define a snow-covered day as one in which the maximum daily snow depth, as calculated by hourly snow depth output of the model, exceeds 1 cm. Most areas in northern Japan and mountainous areas in eastern Japan are covered with snow for more than 100 days (Fig. 7e). Table 3 shows the climatology of snow-covered days from 1961 to 1990 and from 1991 to 2020 at four or five elevation ranges in each region. The climatological number of snow-covered days increases at higher latitudes and elevations. In contrast to SDmax and Sx1d, the number of snow-covered days has been

Table 3 Climatology of snow-covered days at each elevation. Round blanks show ratios of 1991–2020 relative to 1961–1990

Elevation(m)	NJ–JS		NJ–PO		EJ–JS		WJ–JS	
	1961–1990	1991–2020	1961–1990	1991–2020	1961–1990	1991–2020	1961–1990	1991–2020
0–250	139.4	133.3 (0.96)	113.2	107.5 (0.95)	71.7	58.6 (0.82)	20.9	14.2 (0.68)
250–500	158.9	154.5 (0.97)	134.5	130.6 (0.97)	108.4	98.3 (0.91)	51.7	41.4 (0.80)
500–1000	178.7	174.9 (0.98)	164.9	161.7 (0.98)	134.3	128.3 (0.96)	76.8	66.0 (0.86)
1000–1500	202.5	198.8 (0.98)	220.2	218.5 (0.99)	179.6	176.5 (0.98)	102.2	85.8 (0.84)
1500–			350.2	349.7 (1.00)	219.0	216.9 (0.99)		

reduced in most regions in Japan (Fig. 8f and Table 3). In northern Japan, the decrease in snow-covered days in from 1991 to 2020 is less than 5% relative to 1961–1990 at all elevations. In contrast, snow-covered days decreased by 18% and 32% at 0–250 m in eastern and western Japan, respectively. In western Japan, snow-covered days decreased by 16% even at elevations higher than 1000 m. Our results indicate that rapid decreases in snow-covered days have already occurred in eastern and western Japan.

4 Discussion

4.1 Trends of background atmospheric conditions during heavy daily snowfall events over coastal areas along the Japan Sea in central Japan

Here, we will show the example of the composite analysis of heavy daily snowfall events on the Japan Sea coast in central Japan, where the heavy snowfall is frequency brought by the JPCZ. Fukui City is a prefectural capital located on this area and has experienced heavy snowfall in early February 2018. The 3-day total snowfall was 129 cm, and the maximum snow depth was 147 cm, which was the greatest snow depth since 1981. Figure 11 shows composites of precipitation, surface wind, and SLP when Sx1d events occur at a grid point near the Fukui observational station. The northeastern wind converges to the east of the Korean Peninsula, and the precipitation band, elongating from northwest to southeast over the western part of the Japan Sea, corresponds to the JPCZ. A large amount of precipitation is calculated around Fukui, most of which is snowfall over land (figure not shown).

Figure 12 shows linear trends of daily precipitation, snowfall, and rainfall from 1959 to 2020 when the Sx1d is calculated. Here, snowfall in Fig. 12 is directly calculated using the physical schemes in the NHRCM. Precipitation increases over most regions, although the statistically significant increases are limited in the mountainous areas

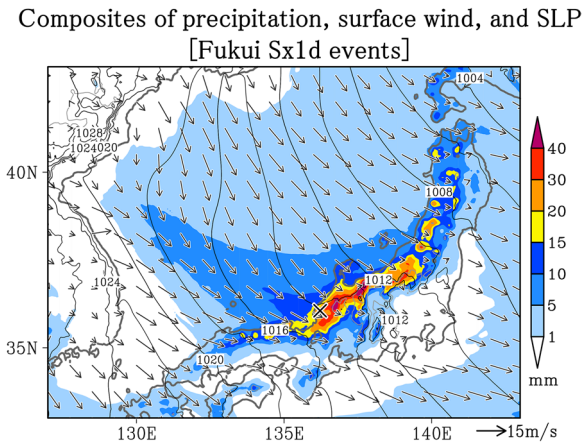

Fig. 11 Same as in Fig. 10a and c, but for Fukui

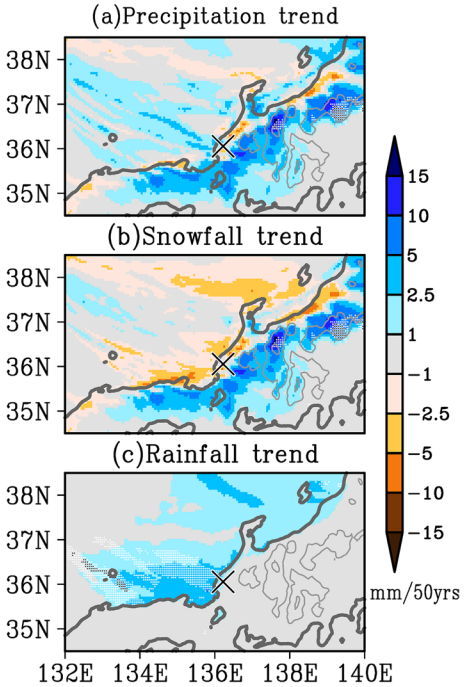

Fig. 12 Linear trends of **a** precipitation, **b** snowfall, and **c** rainfall when Sx1d is calculated by DS5km. White and black dots show statistically significant grids with 90 and 95% confidence levels, respectively. A cross mark represent the location of Fukui

(Fig. 12a). Snowfall, on the other hand, increases over the inland and mountainous areas as with the precipitation, while it decreases over the ocean and coastal areas (Fig. 12b). Rainfall increases over the ocean, which shows statistically significance at the 90% confidence level. Since the composite of air temperature shows above and below 0 °C over the ocean and land, respectively (Fig. 13a), the conversion from snowfall to rainfall has been accelerated due to significant warming (Fig. 13b). Precipitable water vapor exceeds 6 mm around the coastal areas and shows the increasing trends over both the land and ocean (Fig. 13c, d). The increasing trend is statistically significant with a 90% confidence level around the JPCZ. Although this composite analysis only focuses on the Sx1d at the Fukui station, this result is partly consistent with decreases and increases in the Sx1d at lower elevations, i.e., coastal areas, and higher elevations, i.e., mountainous areas, respectively (Figs. 7d and 9c) due to historical warming.

4.2 Factors causing biases of long-term trends

Kobayashi et al. (2015) already pointed out that the global mean temperature in the lower troposphere in JRA-55 showed interannual variations very similar to those in observational data (HadAT2) and comparable with the other reanalysis data, NCEP/NCAR

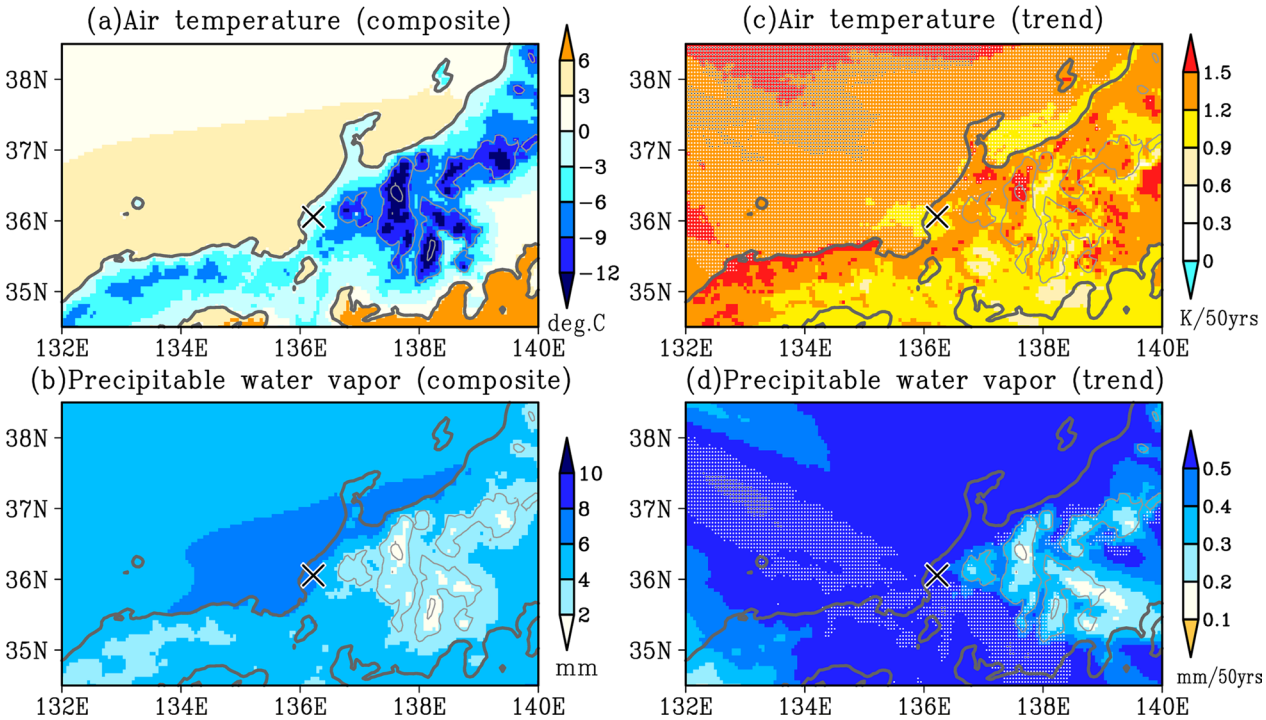

Fig. 13 Composites of surface air temperature and precipitable water vapor and their trends when Sx1d is calculated by DS5km. **a** Surface air temperature and **b** its trend; **c** precipitable water vapor and **d** its trend. White and black dots show statistically significant grids with 90 and 95% confidence levels, respectively

reanalysis and ERA-40. DS5km can be compared directly with the station data in Japan; it indicates that the interannual variations of surface air temperature are quite similar to the observation, even before 1980, in all of Japan (Fig. 4a). The long-term trend is, however, underestimated by DS5km. It is well known that the reproducibility of the reanalysis data itself depends on assimilated observations, especially satellite data. Actually, the quality of JRA-55 has gradually changed from the 1960s to the 2010s (Kobayashi et al. 2015). The underestimation of long-term trends can be caused by an innovation in the satellite data assimilated in JRA-55 around the late 1990s. Our experimental design, excluding land-use changes, such as urbanization and deforestation, can also underestimate the temperature rise in Japan. After 1980, the variation and warming trend are quite similar to those observed. The interannual variations and trends in annual total precipitation are well reproduced by DS5km after the 1980s (Fig. 4b). On the other hand, DS5km has cold temperature biases and positive precipitation biases in the mountainous area in eastern and northern Japan in winter (Figs. 2a, 3b), respectively, which can cause the overestimation of snow accumulation. Moreover, positive snow cover biases can lead to cold bias around the surface. It is difficult to widely evaluate the reproducibility of simulated snow cover because of a lack of observational data.

The annual mean temperature, total precipitation, and maximum snow depth in DS5km can reproduce both interannual and decadal variations (Figs. 4 and 5). The El Niño-Southern Oscillation (ENSO) is a typical interannual variation that influences seasonal temperature and precipitation in Japan. Imada et al. (2021) pointed out that various flavors of ENSO affect summer heavy rainfall in each region of Japan in different ways. Ueda et al. (2014) indicated that the tropical heating relevant to the ENSO cycle, i.e., an enhancement of convection in the vicinity of the Philippines, influenced heavy snowfall on the Japan Sea side via the teleconnection. These points of view can be related to the interannual variations of precipitation (Fig. 4) and snow depth (Fig. 5). Generally, reanalysis data are considered reliable for interannual and shorter-timescale variations, while the availability of longer-timescale variations such as decadal variability is uncertain. Our comparison of DS5km and the site observation suggests that JRA-55 can correctly capture the decadal variations around Japan. On the other hand, the reproducibility of interannual and decadal variations of precipitation extreme indices is worse than that of other

variables. Further experimental designs and simulations are needed to improve them.

5 Conclusions

We conducted a high-resolution dynamical downscaling using NHRCM with 5-km grid spacing forced by the JRA-55 (DS5km). DS5km well reproduced the climatology of the annual mean surface air temperature and annual total precipitation, while air temperature has cold and warm biases in cold and warm seasons, respectively. The DS5km also reproduced recent rapid warming and interannual variations of annual mean air temperature, annual total precipitation, and annual number of heavy precipitation days. The skills of DS5km for simulating air temperature and precipitation are comparable to that of the DSJRA-55. Composite analyses of annual maximum daily snowfall events at Fukui City indicate that heavy daily snowfall is brought about by the JPCZ, and the snowfall amounts show increasing and decreasing trends over mountains and coastal areas, respectively, due to historical warming and moistening.

As compared with DSJRA-55, DS5km has an important advantage in calculating snow depth for all of Japan with 5-km grid spacing. The annual maximum snow depth and annual maximum daily snowfall show significant decreasing trends in eastern and western Japan, while they show increasing trends at higher elevations in northern and eastern Japan. The Pacific Ocean side of northern Japan has a clear elevation dependency of annual maximum snow depth and annual maximum daily snowfall, while the Japan Sea side has no elevation dependency. Long-term dynamical downscaling with a land surface model is useful for evaluating historical changes in snow depth, not only in the plains but also in mountainous areas.

In our experiment, the land uses are fixed from 1958 to 2020. The impact of historical changes in land use will be studied in the future. Also, our dynamical downscaling still has some problems in representing the extreme precipitation. The grid spacing of 5 km is insufficient to simulate deep convections explicitly and resolve complex terrain over Japan, which causes failures in representing heavy precipitations, such as senjo-kousuitai and snowfalls accompanied by winter monsoons. An enhancement of the model's resolutions is necessary. In addition, long-term continuous dynamical downscaling sometimes fails to simulate synoptic-scale environmental conditions, such as typhoon tracks, which results in biases for precipitation and wind extremes. Fukui et al. (2018) showed that a regional reanalysis, assimilating the observations covering long term only, reduces the errors of conventional dynamical downscaling. To evaluate past local climate variations, including extreme states, more appropriately, long-term regional reanalyses would be desired in the future.

Abbreviations

AMeDAS	Automated Meteorological Data Acquisition System
DSJRA-55	Dynamical regional downscaling using the JRA-55 reanalysis
DS5km	Dynamical regional downscaling using the NHRCM with 5-km grid spacing
DS20km	Dynamical regional downscaling using the NHRCM with 20-km grid spacing
ENSO	El Niño–Southern Oscillation
JRA-55	Japanese 55-year reanalysis
NHRCM	Non-hydrostatic regional climate model
nPR100	Annual frequency of daily precipitation exceeding 100 mm/day
RCDSJRA-55	Regional climate downscaling using the JRA-55 reanalysis
aRx1d	Annual maximum daily precipitation
SDmax	Annual maximum snow depth
Sx1d	Annual maximum daily snowfall

Acknowledgements

We thank two anonymous reviewers for their useful comments and suggestions. We thank Dr. Yukiko Imada for discussing interannual and decadal variations in JRA-55. This research was supported by the Integrated Research Program for Advancing Climate Models (TOUGOU) Grant Number JPMXD0717935561 from the Ministry of Education, Culture, Sports, Science and Technology (MEXT), Japan, MEXT-Program for the advanced studies of climate change projection (SENTAN) Grant Number JPMXD0722680734, and JSPS KAKENHI Grant Number 19H01377 and 19H05697.

Author contributions

HK proposed the topics, conducted the numerical simulations, and analyzed the output of the simulations. SF established the experimental design and conducted the numerical simulations. MN and SW analyzed the simulation results. KO conducted the numerical simulation and analyzed the simulation results. AM checked the numerical design. TN and KM supported the gathering and analyzing of observational data. All authors read and approved the final manuscript.

Funding

This research was supported by the Integrated Research Program for Advancing Climate Models (TOUGOU) Grant Number JPMXD0717935561 from the Ministry of Education, Culture, Sports, Science and Technology (MEXT), Japan, MEXT-Program for the advanced studies of climate change projection (SENTAN) Grant Number JPMXD0722680734, and JSPS KAKENHI Grant Number 19H01377 and 19H05697.

Availability of data and materials

Data sharing is not applicable to this article as no datasets were generated or analyzed during the current study. Please contact author for data requests.

Declarations

Competing interests

The authors declare that they have no competing interest.

Received: 21 June 2022 Accepted: 12 January 2023
Published online: 24 February 2023

References

Adachi SA, Kimura F, Kusaka H, Inoue T, Ueda H (2012) Comparison of the impact of global climate changes and urbanization on summertime future climate in the Tokyo metropolitan area. J Appl Meteorol Climatol 51:1441–1454

Beljaars ACM, Holtslag AAM (1991) Flux parameterization over land surfaces for atmospheric models. J Appl Meteor 30:327–341
Berg P, Haerter JO (2013) Unexpected increase in precipitation intensity with temperature: a result of mixing of precipitation types. Atmos Res 119:56–61
Fujibe F (1995) Temperature rising trends at Japanese cities during the last 100 years and their relationship with population, population increasing rates and daily temperature ranges. Pap Meteorol Geophys 46:35–55
Fujibe F (2009) Detection of urban warming in recent temperature trends in Japan. Int J Climatol 29:1811–1822
Fujibe F (2016) Annual variation of extreme precipitation intensity in Japan: assessment of the validity of Clausius–Clapeyron scaling in seasonal change. SOLA 12:106–110
Fukui S, Iwasaki T, Saito K, Seko H, Kunii M (2018) A feasibility study on the high-resolution regional reanalysis over Japan assimilating only conventional observations as an alternative to the dynamical downscaling. J Meteor Soc Japan 96:565–585
Hara M, Yoshikane T, Kawase H, Kimura F (2008) Estimation of the impact of global warming on snow depth in Japan by the pseudo-global-warming method. Hydrol Res Lett 2:61–64
Hatsuzuka D, Sato T, Higuchi Y (2021) Sharp rises in large-scale, long-duration precipitation extremes with higher temperature over Japan. Npj Clim Atmos Sci 4:29
Hirai I, Sakashita T, Kitagawa H, Tsuyuki T, Hosaka M, Oh'izumi M (2007) Development and validation of a new land surface model for JMA's operational global model using the CEOP observation dataset. J Meteor Soc Japan 85A:1–24
Hori ME, Inoue J, Kikuchi T, Honda M, Tachibana Y (2011) Recurrence of intraseasonal cold air outbreak during the 2009/2010 winter in Japan and its ties to the atmospheric condition over the Barents-Kara Sea. SOLA 7:25–28
Ikawa M, Saito K (1991) Description of the nonhydrostatic model developed at the Forecast Research Department of the MRI. Tech Rep MRI 28:23
Imada Y, Kawase H (2021) Potential seasonal predictability of the risk of local rainfall extremes estimated using high-resolution large ensemble simulations. Geophys Res Lett. https://doi.org/10.1029/2021GL096236
Inatsu M, Kawazoe S, Mori M (2021) Trends and projection of heavy snowfall in Hokkaido, Japan, as an application of self-organizing map. J Appl Meteorol Clim 60:1483–1494
Inoue S, Yokoyama K (2003) Estimation of snowfall depth, maximum snow depth, and snow pack environments under global warming in Japan from five sets of predicted data. J Agric Meteorol 59:227–236
IPCC 2021: summary for Policymakers. In: Masson-Delmotte V, Zhai P, Pirani A, Connors SL, Péan C, Berger S, Caud N, Chen Y, Goldfarb L, Gomis MI, Huang M, Leitzell K, Lonnoy E, Matthews JBR, Maycock TK, Waterfield T, Yelekçi O, Yu R, Zhou B (eds) Climate change 2021: the physical science basis. Contribution of working group I to the sixth assessment report of the intergovernmental panel on climate change. Cambridge University Press. In Press
Ishii Y, Suzuki K (2011) Regional characteristics of variation of snowfall in Japan. J Jpn Assoc Hydrol Sci 41:27–37 (**in Japanese with an English abstract**)
Ishizaki NN, Takayabu I, Oh'izumi M, Sasaki H, Dairaku K, Iizuka S, Kimura F, Kusaka H, Asachi SA, Kurihara K, Murazaki K, Tanaka K (2012) Improved performance of simulated Japanese climate with a multi-model ensemble. J Meteor Soc Japan 90:235–254
Japan Meteorological Agency (JMA) (2021) Climate change monitoring report 2020
Kain JS (2004) The Kain-Fritsch convective parameterization: an update. J Appl Meteor 43:170–181
Kain JS, Fritsch JM (1990) A one-dimensional entraining/detraining plume model and its application in convective parameterization. J Atmos Sci 47:2784–2802
Kawase H, Yoshikane T, Hara M, Fujita M, Ishizaki N, Hatsushika H, Kimura F (2012) Downscaling of snow cover changes in the late 20th century using a past climate simulation method over Central Japan. SOLA 8:61–64
Kawase H, Sasaki H, Murata A, Nosaka M, Ishizaki NN (2015) Future changes in winter precipitation around Japan projected by ensemble experiments using NHRCM. J Meteor Soc Japan 93:571–580
Kawase H, Murata A, Mizuta R, Sasaki H, Nosaka M, Ishii M, Takayabu I (2016) Enhancement of heavy daily snowfall in central Japan due to global warming as projected by large ensemble of regional climate simulations. Clim Change 139:265–278
Kawase H, Sasai T, Yamazaki T, Ito R, Dairaku K, Sugimoto S, Sasaki H, Murata A, Nosaka M (2018) Characteristics of synoptic conditions for heavy snowfall in western to northeastern Japan analyzed by the 5-km regional climate ensemble experiments. J Meteor Soc Japan 96:161–178
Kawase H, Iida H, Aoki K, Shimada W, Nosaka M, Murata A, Sasaki H (2019) Comparison of snow cover observations along the Tateyama-Kurobe Alpine route with snow cover simulations using the non-hydrostatic regional climate model (NHRCM) with different horizontal resolutions. J Geogr (chigaku Zasshi) 128:77–92 (**in Japanese with an English abstract**)
Kawase H, Murata A, Yamada K, Nakaegawa T, Ito R, Mizuta R, Nosaka M, Watanabe S, Sasaki H (2021) Regional characteristics of future changes in snowfall in Japan under RCP2.6 and RCP8.5 scenarios. SOLA 17:1–7
Kayaba N, Yamada T, Hayashi S, Onogi K, Kobayashi S, Yoshimoto K, Kamiguchi K, Yamashita K (2016) Dynamical regional downscaling using the JRA-55 reanalysis (DSJRA-55). SOLA 12:1–5
Kitagawa H (2000) Radiation processes. Rep Numer Predict Div 46:16–31 (**in Japanese**)
Kobayashi S, Ota Y, Harada Y, Ebita A, Moriya M, Onoda H, Onogi K, Kamahori H, Kobayashi C, Endo H, Miyaoka K, Takahashi K (2015) The JRA-55 reanalysis: general specifications and basic characteristics. J Meteor Soc Japan 93:5–48
Lenderink G, Van Meijgaard E (2008) Increase in hourly precipitation extremes beyond expectations from temperature changes. Nat Geosci 1:511–514
Lenderink G, Barbero R, Loriaux JM, Fowler HJ (2017) Super Clausius–Clapeyron scaling of extreme hourly convective precipitation and its relation to large-scale atmospheric conditions. J Clim 30:6037–6052
Loriaux JM, Lenderink G, De Roode SR, Siebesma AP (2013) Understanding convective extreme precipitation scaling using observations and an entraining plume model. J Atmos Sci 70:3641–3655
Mizuta R, Murata A, Ishii M, Shiogama H, Hibino K, Mori N, Arakawa O, Imada Y, Yoshida K, Aoyagi T, Kawase H, Mori M, Okada Y, Shimura T, Nagatomo T, Ikeda M, Endo H, Nosaka M, Arai M, Takahashi C, Tanaka K, Takemi T, Tachikawa Y, Temur K, Kamae Y, Watanabe M, Sasaki H, Kitoh A, Takayabu I, Nakakita E, Kimoto M (2017) Over 5000 years of ensemble future climate simulations by 60 km global and 20 km regional atmospheric models. Bull Amer Meteor Soc 98:1383–1398
Murata A, Sasaki H, Kawase H, Nosaka M, Oh'izumi M, Kato T, Aoyagi T, Shido F, Hibino K, Kanada S, Suzuki-Parker A, Nagatomo T (2015) Projection of future climate change over Japan in ensemble simulations with a high-resolution regional climate model. SOLA 11:90–94
Nakanishi M, Niino H (2004) An improved Mellor–Yamada level-3 model with condensation physics: its design and verification. Bound-Layer Meteor 112:1–31
Nakano M, Kato T, Hayashi S, Kanada S, Yamada Y, Kurihara K (2012) Development of a 5-km-mesh cloud-system-resolving regional climate model at the Meteorological Research Institute. J Meteor Soc Jpn 90A:339–350
Sasaki H, Kurihara K, Takayabu I, Uchiyama T (2008) Preliminary experiments of reproducing the present climate using the non-hydrostatic regional climate model. SOLA 4:25–28
Schwalm CR, Glendon S, Duffy PB (2020) RCP8.5 tracks cumulative CO_2 emissions. Proc Natl Acad Sci USA 117:19656–19657
Sellers PJ, Mintz Y, Sud YC, Dalcher A (1986) A simple biosphere model (SiB) for use within general circulation models. J Atmos Sci 43:505–531
Suzuki H (2006) Long-term changes in snowfall depth and snow cover depth in and around Niigata Prefecture from 1927 to 2005: Analysis using data observed at railway stations. Tenki 53:185–196 (**in Japanese with an English abstract**)
Suzuki K (2013) Importance of meteorological observation in the Japanese Alps Region. J Geogr (chigaku Zasshi) 122:553–570 (**in Japanese with an English abstract**)
Ueda H, Kibe A, Saitoh M, Inoue T (2014) Snowfall variations in Japan and its linkage with tropical forcing. Int J Climatol 35:991–998
von Storch H, Langenberg H, Feser F (2000) A spectral nudging technique for dynamical downscaling purposes. Mon Wea Rev 128:3664–3673
Yabu S, Murai S, Kitagawa H (2005) Clear-sky radiation scheme. Rep Numer Pred Div 51:53–64 (**in Japanese**)
Yamaguchi S, Abe O, Nakai S, Sato A (2011) Recent fluctuations of meteorological and snow conditions in Japanese mountains. Ann Glaciol 52:209–215

Publisher's Note